lake depth and vertical diffusion (1.29); by rearranging the terms, the river flow can be given as a function of the longitudinal length *x*=L (1.35).

$$u = \frac{xD}{H^2}$$
$$Q = uWH = \frac{LDW}{H} \qquad (1.35)$$

Where L is the length of influence, W is the lake width, and Q is required river flow. Letting *L* equal the distance from the Cedar mouth to MWY (15,000 meters), setting H equal to the mean depth (35 meters), and W equal to the width (3,000 meters). The vertical eddy diffusion can range in value, in 2004 eddy diffusion ranged from 0.2 (cm/s) to 50 (cm/s) (Table 2. 11).

For the range of eddy diffusion, the required Cedar flow rate would range between 25 and 6400 (m^3/s) and travel time would range between 730 to 2.8 days: travel from the Cedar mouth to MWY (Table 1. 19). In 2004 the mean river flow was about 17 (m^3/s) and about 21 (m^3/s) for mean plus one standard deviation (Table 1. 15). At this flow, the eddy diffusion must be less than 0.2 (cm/s) and the travel time to MWY would be greater than 730 days. From the Wedderburn Number and temperature analysis (§1.3.3), the isotherm response ranged from about five to 10 days, which is much less than the 730 days; only flows near 1800 (m^3/s) approach the observed response times (Table 1. 19).

Table 1. 19. Estimated flow rates and time scales that could produce the longitudinal isotherm adjustments observed in Lake Washington. Travel was defined as the distance from the Cedar mouth to the MWY location.

Eddy Diffusivity (cm^2/s)	Flow Rate (m^3/s)	Travel Time (days)
0.2	25	730
14	1822	10
50	6402	2.8

The Advective-Diffusion solution shows the Cedar River effect decays exponentially and that a river flow of 1800 (m^3/s) is required to influence the longitudinal isotherm structure under the time scales observed (Table 1. 19). Such a flow condition was 100 times greater than the mean flow for the observation time period (Table 1. 15). For the mean flow plus one standard deviation, the Cedar would influence lake dynamics to about 200 meters from the mouth. These two results corroborate the

very small correlations between the Cedar River temperature flux and temperature response at SWA (Table 1. 16). The three analyses show the Cedar River had negligible influence on the temperature observations at SWA.

1.4 Discussion/Conclusion

In years 2003 and 2004 during the early spring, the longitudinal isotherm response to wind conditions was investigated. The Wedderburn Number (W_N) was used to assess the dynamic balance between wind stress and longitudinal baroclinic pressure gradient, which is manifested by a tilted isotherm structure. Use of the Wedderburn was affirmed by a Principal Component Analysis of isotherm and velocity structure and response. The eigenvector shapes and expansion coefficients had a form and response that is characteristic of first mode vertical and first mode horizontal wave; their form and response was cross-validated against observed isotherm and velocity responses. The first mode expansion coefficients expressed the same temporal evolution as the average density time series. The relative difference of the average density at the north and south ends of the lake corresponded to a tilted isotherm structure, which was corroborated by synoptic SCAMP temperature profiles and subsequent longitudinal temperature contours.

The W_N and wind stress analysis showed the isotherm response was a forced response from surface wind stress; the internal seiche was not allowed to freely oscillate. As a result, the direction of isotherm tilt and duration depended on the direction and duration of the wind; the amount of tilt depended on the magnitude of the surface wind stress and vertical stratification and is expressed in W_N. The Cedar River was not a significant contribution to the observed isotherm response. During the time of observation, the lake was weakly stratified and affected internal seiches with periods of oscillation larger than the periodicity of the wind events. Because the density adjustment time scales were greater than the periodicity of the wind events, the observed wind stress maintained the isotherms in a tilted position for time intervals in the range of 10 to 18 days.

Over the time of observation, incident solar radiation increased and warmed the surface of the lake. Concurrently, nearly 70% of the time winds were northward and blew the warmer surface layer to the north end of the lake; the persistent northward

direction was able to maintain a longitudinal density gradient for intervals of 10 to 18 days. The relatively small Wedderburn Numbers showed wind stress was sufficient to overcome the stratification, and induce significant tilting of the isotherms. Under these conditions, significant vertical mixing occurs at the downwind end and bottom water upwells at the upwind end (Stevens and Imberger, 1996; Imberger and Patterson, 1990, Stevens et al, 1996). The longitudinal SCAMP temperature profiles showed isotherms tilted to the bottom of the lake at the downwind end with corresponding surfacing of the isotherms at the upwind end. Concurrent fluorescence readings showed uniform profiles to the bottom at the downwind end and much shallower profiles at the upwind end. Such a gradient in the mixing depth would create significantly different habitat conditions along the length of the lake. The most relevant condition would be the integrated amount of light phytoplankton would experience; the depth-integrated photosynthesis would be much less for the deeper mixing areas.

The duration of the longitudinally varying mixing depth, 10 to 18 days, is comparable to the e-folding time (14 days) of the dominant phytoplankton *Aulacoseira subarctica* (Gibson and Foy, 1993). The physical conditions persist long enough to affect two generations. At the north end, the phytoplankton could experience a lower photosynthesis rate compared to phytoplankton at the south end. If nutrient and temperature differences could not compensate for the photosynthesis differences, then the isotherm tilt could affect the ecological community that develops during the early-spring period.

2 Effect of Isotherm Tilt and Hydrodynamics on the Early-Spring Diatom Bloom

2.1 Introduction

In Section One, it was shown that persistent northward winds produced a persistent upward isotherm tilt from north-to-south; this tilt created a variable mixed layer depth that increased from south to north. In this section, I investigate how the persistent isotherm tilt and associated vertical eddy diffusion affected the diatom population during the early spring bloom. During the tilt, the mixing depth is deeper at the north end of the lake where the depth-integrated photosynthesis rate is less than in the central and southern parts of the lake, which have shallower mixing depths. At the south end of the lake, upwelling dilutes the phytoplankton and the corresponding winds produce surface flows that transport the population downwind; phytoplankton are diluted and transported out of the region faster than they can grow. The tilt and associated hydrodynamics create better growth conditions in the central part of the lake. These better conditions allow the larger observed biomass at MWY compared to NOA and SWA.

Light, temperature, and nutrients are important environmental variables that affect phytoplankton growth and species succession (Foy and Gibson, 1993; Sebastian, Interlandi, and Kilham, 2001; Arhonditsis, Winder, Brett, and Schindler, 2004; Sommer, 1994), and differences in these variables cause spatial and temporal differences in species composition and density (Felip and Catalin, 2000; Barbiero et al., 2000). Changes in vertical mixing depth can be an important dimension in determining species compositions (Wall, Briand, and Ottawa, 1980; Viner and Kemp, 1983). The physical structure of the lake (stratification, flow, and mixing) affects the amount of light, temperature, and nutrients that phytoplankton may experience in the water column.

Wind and stratification affect the amount of isotherm tilt, which will be more dramatic during the spring when density differences are small and small barotropic tilts can

create large baroclinic responses. At the ends of the lake, the isotherm tilt creates two different environments. At the downwind end above the density interface, vertical mixing is enhanced from vertical velocity shears, gyres, and horizontal dispersion; the density interface suppresses mixing below the interface (Stevens and Imberger, 1996; Farrow and Stevens, 2003). Because mixing is suppressed below the density interface and because of the upward tilt, mixing is constrained higher in the water column at the upwind end. At the upwind end, surface water is advected downwind and is replaced by sub-surface water that is lifted up to the surface where it is turned around and transported downwind (Monismith, 1986; Imberger and Patterson, 1990).

In this Section, I show that the tilt affects the depth-integrated photosynthesis rate, which governs phytoplankton kinetics at NOA, and that upwelling conditions govern growth at SWA. Using a one-dimensional advective/reactive diffusion model, I show that the eddy diffusion vertical distribution and magnitude affects the success of the phytoplankton bloom; such a condition was hypothesized by Arhonditsis, Winder, Brett, and Schindler (2004) as a possible effect on the phytoplankton bloom.

2.2 Methods

2.2.1 Field Methods

To investigate effects of eddy diffusion and mixing depth on the phytoplankton population, eddy diffusion and phytoplankton densities must be measured along the depth of the water column. When numerous measures are required for the vertical density of phytoplankton, fluorescence profiles are typically used as a surrogate method to quantify total biomass, but the method cannot distinguish species shifts. In this study, a particle analyzer was used to quantify phytoplankton densities as biovolume concentration and particle size. Quantitative phytoplankton analyses were also performed to determine species composition and biovolume, which were correlated to the particle analyzer results. Vertical profiles of eddy diffusion were determined from temperature micro-structure profiles obtained from the SCAMP.

In situ particle sizes and concentrations were measured with a Sequoia Instruments Laser In Situ Scattering Transmissometer (LISST-100) particle analyzer, which can measure particle sizes from 2.5 to 500 μm. The LISST has been successfully used

to measure vertical profiles of phytoplankton and quantify effects of horizontal transport on phytoplankton concentrations (Serra et al., 2001; Serra et al., 2003). The LISST-100 was configured for a sampling rate of 3 Hz. The SCAMP was configured with a Li-Cor LT-192SA Photosynthetically Active Radiation sensor, a Fluorometer sensor with a 455 nanometer excitation diode, and two channels for fast temperature measurements at a 100 Hz sample rate; temperature-gradient response was calculated internally (Precision Measurement Engineering [PME], 2000). Each temperature channel was equipped with a FP07 glass thermistor manufactured by Thermometrics, Inc. The FP07 thermistor has an operating range between 0 ^{o}C and 30 ^{o}C with an accuracy of 0.05 ^{o}C and a resolution of 0.001 ^{o}C. The SCAMP was calibrated for a descent rate of about ten cm/sec.

Complementing the LISST-100 and SCAMP data, quantitative phytoplankton samples were collected bi-weekly in 2003, and bi-weekly pre-bloom and weekly during the diatom bloom in 2004 (the bloom was determined when fluorescence doubled from the pre-bloom fluorescence). Samples were collected at the NOA, MWY and SWA locations with a ten-plus meter length of 1.6 cm (ID) diameter plastic tube lowered through the water column; the tube was marked at ten meters so the sampler collected water from the upper ten meters (King County, 2004). The collected water was emptied into a clean HDPE container and mixed thoroughly; from this mixture, a 60 ml sample was extracted, preserved with Lugol's solution, capped, and tightly wrapped with aluminum foil. All samples were kept cool prior to shipping to WATER Environmental Services, Inc. for microscopic analyses.

Taxonomic analysis was performed on a single 1.0 ml subsample of each well-mixed lake sample using a Sedgewick-Rafter counting chamber and Leitz compound microscope (@100X, 400X magnification). A transect counting methodology was used in which successive horizontal sweeps of the S-R chamber were made under 100X power so that at least one half of the volume of each 1 ml subsample was counted. The entire 1 ml S-R chamber was analyzed to enumerate rare and very large forms, like *Ceratium* sp. Only algal cells presumed to be alive at the time of sampling (chloroplast reasonably intact in preserved sample) were counted. Average counts for each phytoplankton taxon were computed from subsample

results, using appropriate multiplying factors. Algal densities were typically reported in natural units as numbers of cells or colonies per ml.

For each sample, cell dimensions of at least five organisms of each phytoplankton were computed to obtain average cell volume per taxon based on geometric shape. Cell volumes for each taxon were calculated for each lake sample analyzed. Determination of cell volume dimensions and identifications were made with a calibrated whipple disc at 400X (high dry magnification) using a Palmer-Maloney nanoplankton chamber (0.1 ml volume) or at 1000X (oil immersion). Cell volumes were reported as cubic microns per ml, and were converted to cubic millimeters per liter (mm^3/L) for report presentation. Species identifications were made primarily according to Prescott (1975, 1980), Patrick and Reimer (1966, 1975), Smith (1950), and Wehr and Sheath (2003).

Nitrogen, phosphate, silica, and chlorophyll *a* data were obtained from the King County Environmental Laboratory, which collects and analyses Lake Washington water samples as part of the Major Lakes Program (King County, 2005). Quantitative zooplankton data was obtained from the University of Washington Zoology Department (Schindler, 2004).

2.2.1.1 Calculation of Eddy Diffusion from Temperature Micro-structure

The Advective/Reactive Diffusion equation requires a value for eddy diffusion, which was determined from energy dissipation by (2.1) (Osborn, 1980).

$$K_e = \frac{\gamma \varepsilon}{N^2} \qquad (2.1)$$

Where K_e is eddy diffusion, γ is the mixing efficiency, ε is energy dissipation, and *N* is the buoyancy frequency. Energy dissipation was determined from the temperature gradient spectrum based on findings from Bachelor (1958) and an analytical form for the spectrum by Gibson and Schwarz (1963). Temperature micro-structure and temperature gradient profiles were obtained with the SCAMP.

In processing the temperature gradient signal, methods followed guidelines suggested by Bill Shaw (2006); his methods were a slight variation of the methods outlined by Fozdar et al. (1985) and Ruddick and Anis (2000). The gradient signal

was first filtered with a 30 Hz second-order Butterworth filter provided by PME (2002). This signal was separated into segments based on changes in the Signal to Noise Ratio (Bill Shaw, 2006) in which a value of -3 dB identified segment breaks, but segment lengths were constrained to a minimum of 246 samples and a maximum of 512 samples (a sample is a single observation). The sample sizes represented a segment length of about 25 cm (256) and 50 cm (512) assuming a ten cm/s descent velocity. Next, each segment was linearly detrended before estimating the power spectral density (PSD). A sine Multi-Taper method with five tapers was used for estimating the PSD (Riedel and Sidorenko, 1995). The spectrum was sharpened by the transfer function for the FP07 thermistor (Fleury and Luek, 1999); the sharpened spectrum was retained for frequencies less than 30 Hz for estimating energy dissipation (Bill Shaw, 2006). This cut-off removes results that are beyond the response time of the FP07 thermistor, which is approximately 20 Hz (PME, 2000).

Energy dissipation was estimated by fitting the theoretical Bachelor spectrum to the obtain spectrum using a Maximum Likelihood Estimator (MLE) (Ruddick and Anis, 2000) modified by Shaw (2006). The algorithm performed two searches (coarse and fine) for the Bachelor wave number (2.2) and Chi (2.2) that provided the optimal MLE.

$$k_B = \left(\frac{\varepsilon}{\nu \kappa_T^2} \right)^{1/4} \tag{2.2}$$

where k_B is the Bachelor wave number, ν is the kinematic viscosity, and κ_T is the thermal molecular diffusion for water.

$$\chi_\Theta = 6\kappa_T \int_0^\infty (S_{obs} - S_n) dk \tag{2.3}$$

Where χ_θ is the integrated temperature gradient spectrum (S_{obs}) corrected for thermistor noise (S_n), and k is the wave number; see Gibson and Schwarz (1963) for elaborations on the relation between energy dissipation, Bachelor wave number, and the integrated temperature gradient.

For the coarse routine, a range of wave numbers ($20 \leq k_B \leq 800$ 1/m) and Chi ($-1+\log_{10}(\chi_\theta)$ to $1+\log_{10}(\chi_\theta)$) were defined and searched over, from which a smaller range was selected for the fine routine; the smaller range was defined as those k_B

and Chi sets that were within 10% of the coarse optimum MLE. The fine routine searched through the minimum and maximum of the retained coarse results. From the fine routine, the optimum k_B and χ_θ were retained for creating the theoretical Bachelor spectrum. The theoretical spectrum was compared to the observed spectrum and each segment was visually inspected for acceptance using two acceptance criteria: the Bachelor spectrum was adequately contained within the 95th confidence intervals of the estimated spectrum, and the temperature gradient series had a signal appropriate to the expected spectral shape (at least the Komolgorov wave lengths were visible in the temperature gradient series). If each spectral fit satisfied these criteria, the energy dissipation value was retained for estimating eddy diffusion (Figure 2. 1 and Figure 2. 2).

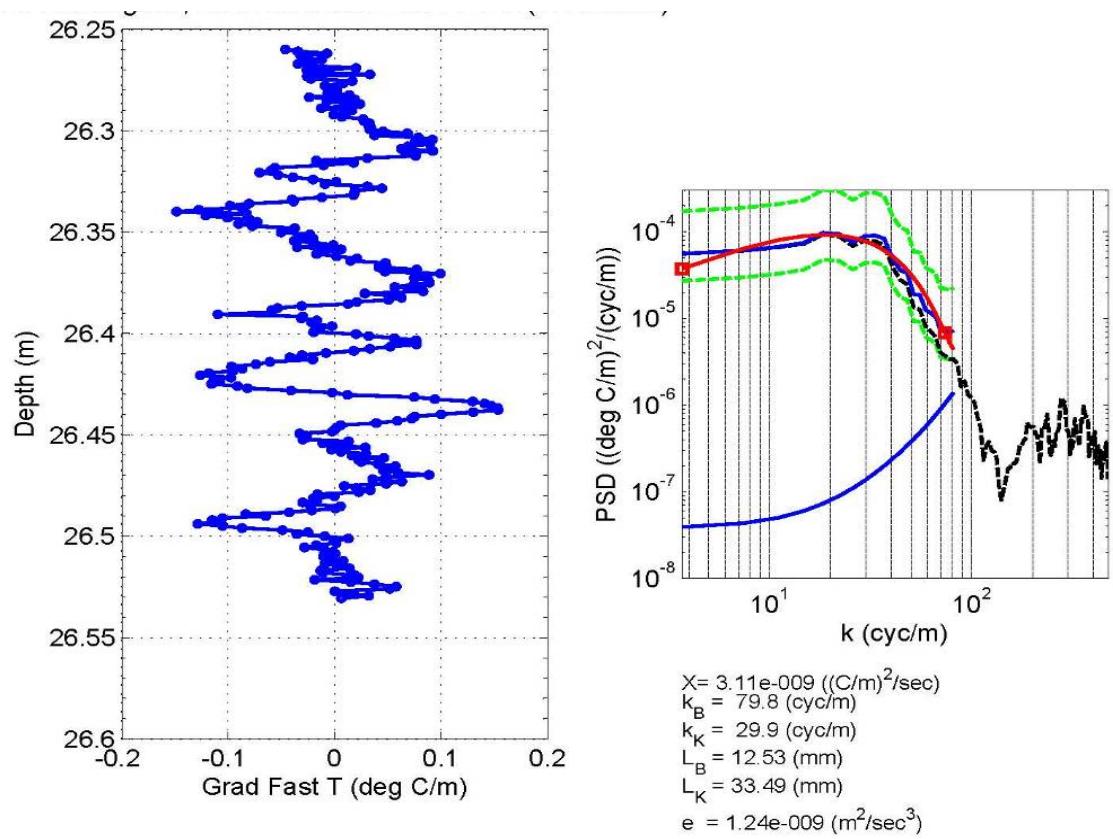

Figure 2. 1. An acceptable fit between theoretical Bachelor spectrum (red line) and the sharpened spectrum (blue line) with 95th confidence intervals (green dashed line). The sharpened spectrum is little affected by noise (lower blue line) and lies just above the unadjusted spectrum (black dashed line). The temperature gradient signal has a wave structure with small undulations about 2 to 4 cm in length, which corresponds to the Kolmorgorov length (L_K = 3.3 cm); eddies at the Bachelor scale would be superimposed on L_K and of length near 1.2 cm. The observed segment has an energy dissipation of 1.2×10^{-9} (m^2/s^3) and Chi of 3.1×10^{-9} ($^oC/m)^2/s$.

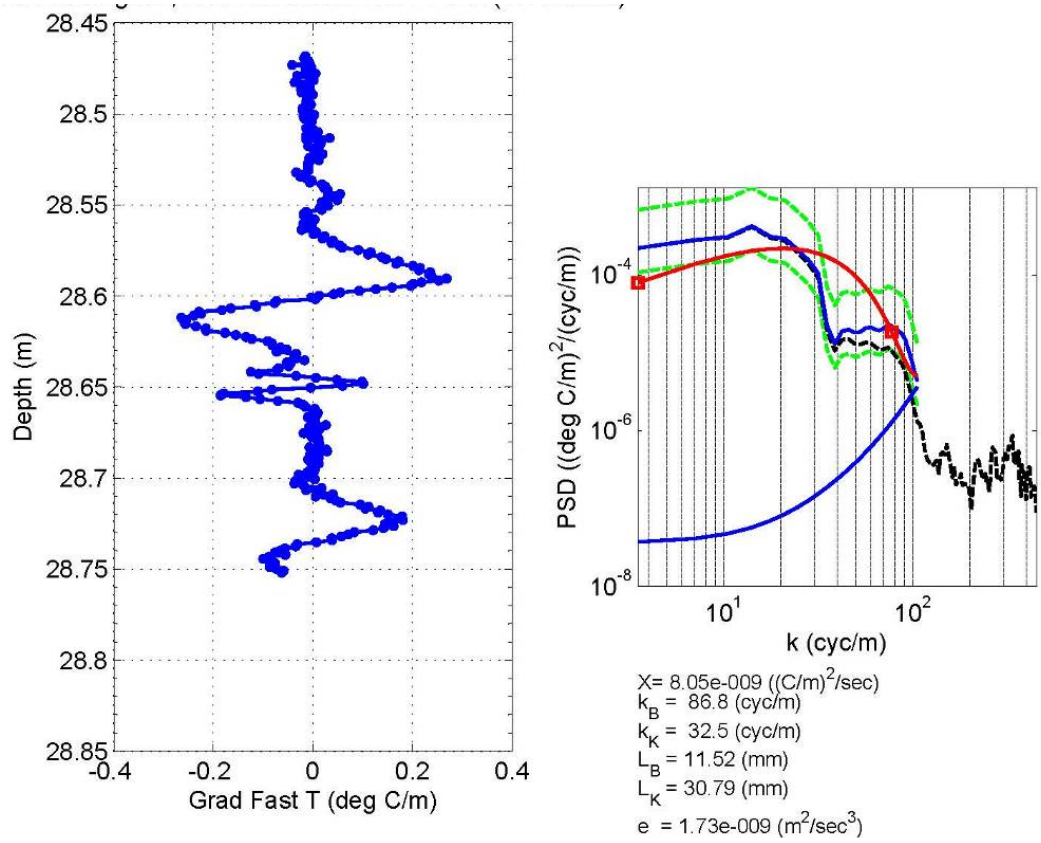

Figure 2. 2. An unacceptable fit between theoretical Bachelor spectrum (red line) and the sharpened spectrum (blue line) with 95th confidence intervals (green dashed line). The sharpened spectrum is slightly affected by noise (lower blue line) and lies just above the unadjusted spectrum (black dashed line). The Bachelor spectrum lies too much outside the 95th confidence intervals of the adjusted spectrum.

After energy dissipation profiles were calculated for each of the two thermistor profiles, the results were averaged into a single segment profile. From the average energy dissipation profile, eddy diffusion was estimated for each segment (2.1) subject to the requirement that $\varepsilon > 15\nu N^2$; otherwise $\varepsilon = 0$ (Itsweire et al., 1993). Mixing efficiency (2.4) was estimated from methods developed by Ivey et al. (1998) as described by (2.5) to (2.11) with the condition that $R_f \leq 0.28$.

$$\gamma = \frac{R_f}{1 - R_f} \tag{2.4}$$

Where R_f is the flux Richardson number.

$$R_f = \left(\frac{\mathrm{Re}_T - 15}{60}\right)\frac{1}{1 + 2.5Fr_T^2} \quad 15 \leq \mathrm{Re}_T \leq 75 \text{ and } Fr_T \geq 1 \tag{2.5}$$

$$R_f = \frac{1}{1+2.5Fr_T^2} \quad \mathrm{Re}_T > 75 \text{ and } \mathrm{Fr_T} \geq 1 \tag{2.6}$$

$$R_f = 0.0047\left(\mathrm{Re}_T - 15\right)\left(\frac{Fr_\gamma - \sqrt{15}}{\sqrt{\mathrm{Re}_T} - \sqrt{15}}\right) \quad 15 \leq \mathrm{Re}_T \leq 75 \text{ and } Fr_T < 1 \tag{2.7}$$

$$R_f = 0.28\left(\frac{Fr_\gamma - \sqrt{15}}{\sqrt{\mathrm{Re}_T} - \sqrt{15}}\right) \quad \mathrm{Re}_T > 75 \text{ and } Fr_T < 1 \tag{2.8}$$

$$Fr_T = \left(\frac{L_O}{L_C}\right)^{2/3} \tag{2.9}$$

$$\mathrm{Re}_T = \left(\frac{L_C}{L_K}\right)^{4/3} \tag{2.10}$$

$$Fr_\gamma = \left(\frac{L_O}{L_K}\right)^{2/3} \tag{2.11}$$

Where $L_O = (\varepsilon/N^3)^{1/2}$ is the Ozmidov scale, $L_K = (\nu^3/\varepsilon)^{1/4}$ is the Kolmogorov scale, and L_C is the centered displacement scale that represents the dimensional scale of overturns or eddies (Imberger and Boashash, 1986). L_C was calculated with instrument software provided by the SCAMP manufacturer; L_C is the Thorpe displacement scale but displaced by moving it vertically by one-half of the displacement value, which locates the displacement at the center of the overturn event.

Buoyancy was estimated for each segment. Contiguous eddy diffusion segments were averaged to obtain a single eddy diffusion segment of equivalent length (Figure 2. 3); averaging weights were based on the segment length.

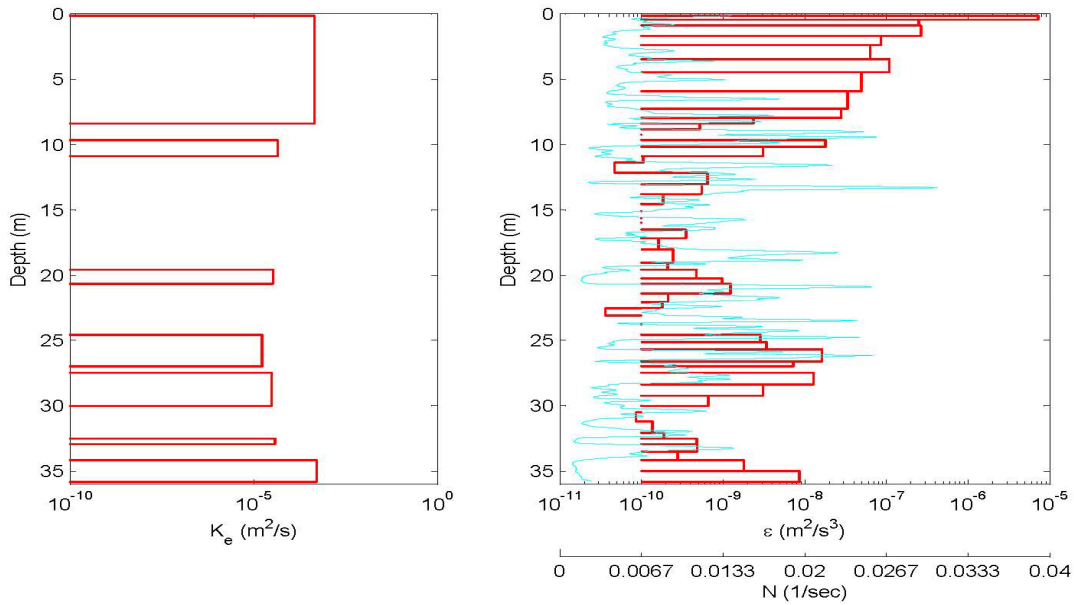

Figure 2. 3. Averaged eddy diffusion segments (K_e, red bars) obtained from average energy dissipation segments (ε, red bars) and buoyancy frequency (N, cyan line) for NWA on Apr. 13, 2004. The average energy dissipation was obtained from the two FP07 thermistors. The bars indicate regions where mixing is active or measurable, the length of the bar represents the magnitude of mixing (K_e) or energy dissipation (ε), and the width of the bars represents the depth of turbulent activity.

2.2.2 Transport and Kinetic Equations

Phytoplankton growth was described with the Advective/Reactive-Diffusion equation (2.12).

$$\frac{\partial c}{\partial t}+u\frac{\partial c}{\partial x}+v\frac{\partial c}{\partial y}+w\frac{\partial c}{\partial z}=\frac{\partial}{\partial x}K_x\frac{\partial c}{\partial x}+\frac{\partial}{\partial y}K_y\frac{\partial c}{\partial y}+\frac{\partial}{\partial z}K_z\frac{\partial c}{\partial z}+\mathrm{g}_{\mathrm{net}}c \qquad (2.12)$$

Where c is phytoplankton concentration, u, v, and w are velocities in respective directions x, y, and z; K_i is eddy diffusivity; and g_{net} is the net phytoplankton growth rate. Limiting interests along the longitudinal (x) and vertical (z) directions and assuming a well-mixed lateral (y) condition, then all $\partial/\partial y=0$.

In a lake forced by a wind such that the Wedderburn Number is small, the upwind and downwind ends will experience horizontal and vertical velocities whereas the interior is driven by horizontal velocities; at the upwind end, vertical velocities bring interfacial and/or hypolimnetic water to the surface (Monismith, 1986; Farrow and Stevens, 2003). Under these conditions at the ends, the vertical velocity term includes upwelling and sinking (2.13).

$$\frac{\partial c}{\partial t}+u\frac{\partial c}{\partial x}+\left(w-w_s\right)\frac{\partial c}{\partial z}=\frac{\partial}{\partial x}K_x\frac{\partial c}{\partial x}+\frac{\partial}{\partial z}K_z\frac{\partial c}{\partial z}+\mathrm{g}_{\mathrm{net}}c \qquad (2.13)$$

Where w_s is the phytoplankton sinking velocity.

The relative importance of each term can de determined by casting the variables in non-dimensional terms in (2.14) that are substituted into (2.13) and give (2.15) (Kundu, 1990; O'Brien and Wroblewski, 1973).

$$\begin{aligned} &x=x'L;\quad y=y'L;\quad z=z'H;\quad t=t'T;\quad u=u'U;\\ &v=v'U;\quad w-w_s=w'W;\quad c=c'C \end{aligned} \qquad (2.14)$$

Where the primed variables are the non-dimensional terms, L is a characteristic length scale, H is a characteristic depth scale, U is a characteristic horizontal velocity scale, W is a characteristic vertical velocity scale, and C is a characteristic concentration scale.

$$\begin{aligned} &\frac{t_U}{T}\frac{\partial c'}{\partial t}+u'\frac{\partial c'}{\partial x}+\frac{t_U}{t_W}w'\frac{\partial c'}{\partial z}=\frac{t_U}{t_{K_X}}\frac{\partial^2 c'}{\partial x^2}+\frac{t_U}{t_{K_Z}}\frac{\partial^2 c'}{\partial z^2}+\frac{t_U}{t_G}c'\\ &t_W=\frac{H}{W};t_U=\frac{L}{U};t_G=\frac{1}{(g_{net})};t_{K_Z}=\frac{H^2}{K_Z};t_{K_X}=\frac{L^2}{K_X} \end{aligned} \qquad (2.15)$$

Where the t_i is a time scale representing vertical transport (W), horizontal transport (U), vertical diffusion (K_Z), horizontal diffusion (K_X), or growth (G).

The horizontal terms can be neglected when growth time scales are less than horizontal transport time scales ($t_G<t_U$). Horizontal velocity will transport phytoplankton along the same light level unless vertical velocity is also present in which down-welling or upwelling will occur. For horizontal time scales (t_U) greater than t_G, one might expect an e-folding (e^1 = 2.72) increase in the phytoplankton population over a distance $L_U=Ut_U$. If the phytoplankton travels a distance L_U before down-welling, significant growth would occur within length L_U; this type of process may be controlling near-shore oceanic phytoplankton blooms (Botsford et al., 2006) and the scaling method has been used for assessing adequate modeling domain scales for simulating spatial phytoplankton response (Hillmer and Imberger, 2007). Therefore, neglecting horizontal terms, one obtains the Peclet (Pe) and Growth (G) Numbers used by O'Brien et al. (2003) (2.16).

$$\frac{t_W}{T}\frac{\partial c'}{\partial t} + w'\frac{\partial c}{\partial z} = \frac{1}{Pe}\frac{\partial^2 c'}{\partial z^2} + Gc'$$

$$G = \frac{t_W}{t_G} = \frac{(g_{net})H}{W} \qquad (2.16)$$

$$\frac{1}{Pe} = \frac{t_W}{t_{K_Z}} = \frac{K_Z}{WH}$$

When Pe is large, phytoplankton sink out of the water with velocity w_s unless growth is sufficient to overcome the sinking; G must increase with increasing Pe. When Pe is small the water column is well mixed by eddy diffusion and phytoplankton will decay exponentially unless growth can supersede the decay; G must exceed one for all Pe sufficiently small (Figure 2. 4 from O'Brien et al., 2003). These two conditions assume the sinking velocity is much larger than the ambient vertical velocity.

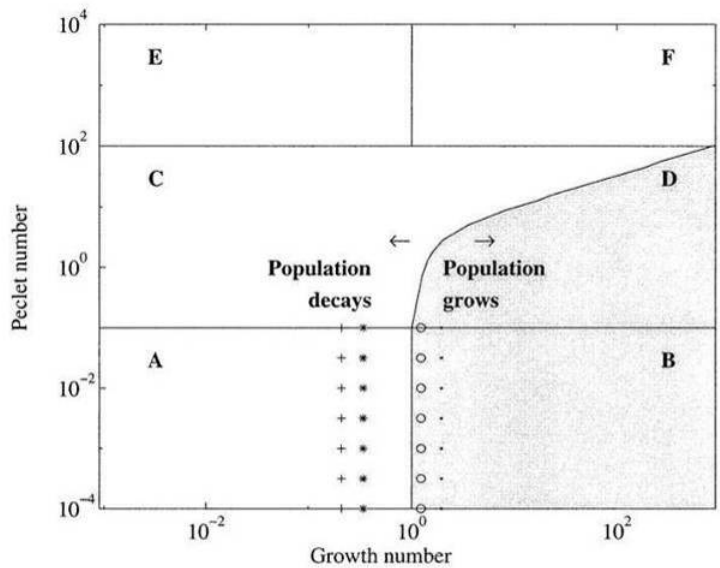

Figure 2. 4. Growth regimes predicted by the advective/reactive diffusion equation for phytoplankton initially uniform in the vertical for sinking rate w_s and mixing depth H. The shaded region of the plot indicates where phytoplankton populations will grow over time. In the unshaded areas, populations will decay. The six growth regimes are defined: (A) exponential decay over time, (B) exponential growth, (C,D) as Pe increases so must G to compensate for sinking, (E) decays monotonically over time, and (F) biomass increases initially but decays completely by time t_s=H/w_s, (reproduced from O'Brien et al. 2003).

The vertical velocity is significant when upwelling occurs at the upwind end of the lake where the upwelled water is turned around and transported downwind (Monismith, 1989; Farrow and Stevens, 2003; Verhagen, 1994). For a particular numerical modeling study of the upwelling region, Farrow and Stevens (2003) found

vertical velocities were greatest in the upper 30% of the water column and horizontal velocities showed a sharp gradient from the surface downward; however this relation could change with different wind and stratification conditions. Because vertical velocity was not measured, upwelling and downwind transport conditions were approximated from observed wind speeds.

Upwelling conditions are a complicated process but a simplified method was developed for a multi-layer box model (Figure 2. 5). Water that is transported downwind is replaced by water from below, this process is depicted as a horizontal velocity in each layer that is redirected vertically upward (Figure 2. 5b). Horizontal flow from each layer adds to the vertical flow, which increases towards the surface. This upward transport dilutes upper cells with water and phytoplankton from lower cells. Eventually, the upwelled water is turned around and transported downwind. This whole process is approximated by a vertical advection term (2.17). Because the velocities are a response to the surface wind stress, the vertical velocity was assumed proportional to the friction velocity (2.17). An exponential distribution was used to approximate the friction velocity distribution, assuming a logarithmic profile applies near the air-water boundary (2.18), which has similar form to that used by Vergahan (1994). Substituting (2.18) into (2.17) gives (2.19); the negative sign accounts for the way the model computes the vertical gradient term. This extra velocity term acts as an additional loss term for phytoplankton that are lifted up from below, turned around and transported downwind; phytoplankton is diluted by upwelled water and advected out of the area. The final form of the Advective/Reactive Diffusion equation is given by (2.20), which was used for the SWA location.

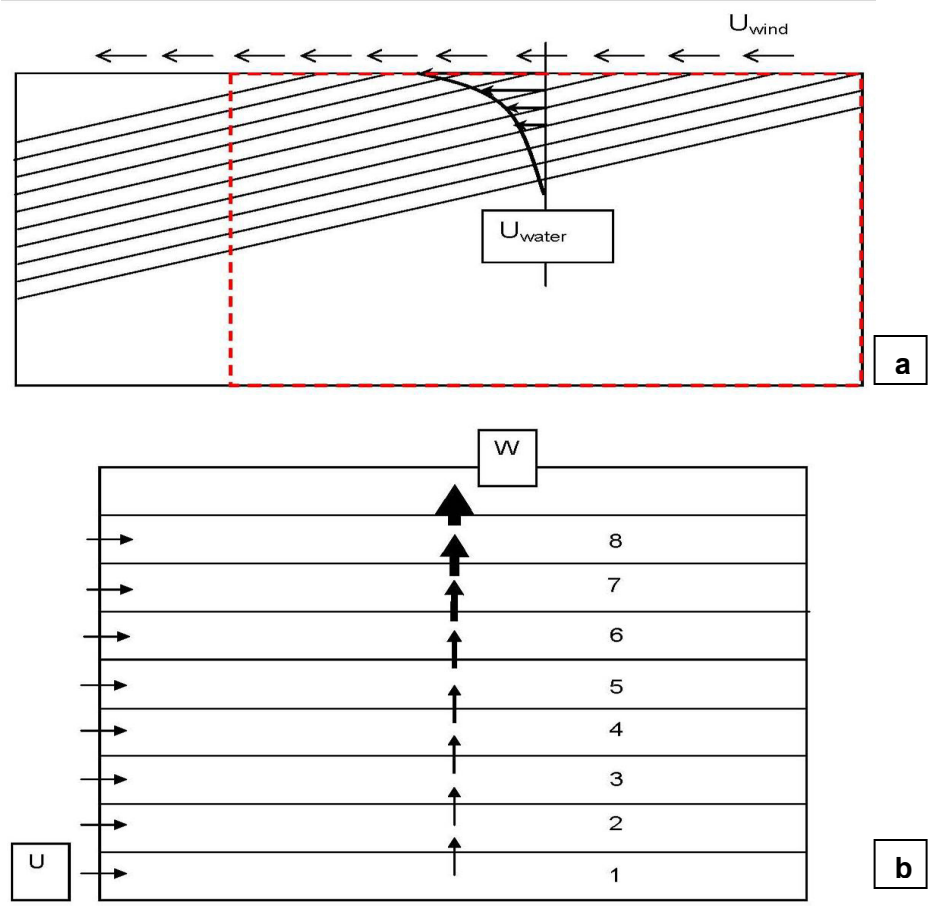

Figure 2. 5. Simple hydrodynamic representation of upwelling and downwind advection that occurs at SWA (a). Upwelling and horizontal transport in the red dashed box (a) is approximated by the multi-layered box in (b). The horizontal (U) and vertical (W) velocities are driven by the surface wind (U_{wind}); vertical velocity increases towards the surface ($W_1<W_2<\ldots<W_8$) as more flow from each layer is upwelled. The vertical velocity distribution was approximated by an exponential distribution.

$$\frac{\partial c}{\partial t} \approx W(z)\frac{\partial c}{\partial z}$$
$$\frac{\partial c}{\partial t} \approx \alpha\, u_*(z)\frac{\partial c}{\partial z} \qquad (2.17)$$

Where c is concentration, W(z) is a variable vertical velocity, α is a calibration coefficient, and u_* is the friction velocity.

$$u_*(z) = u_*^o \exp(-\beta z) \qquad (2.18)$$

Where u^o_* is the friction velocity at the water surface and β is a decay parameter, which depends on the fetch length but is assumed to integrated fetch effects over the model domain.

$$\frac{\partial c}{\partial t} \approx -\alpha u_*^o \exp(-\beta z)\frac{\partial c}{\partial z} \qquad (2.19)$$

$$\frac{\partial c}{\partial t} + \left(w_s - \alpha u_*^o \exp(-\beta z)\right)\frac{\partial c}{\partial z} = \frac{\partial}{\partial z} K_z \frac{\partial c}{\partial z} + \mathrm{g}_{\mathrm{net}} c \qquad (2.20)$$

The velocity and eddy diffusion terms determine how physics affects population dynamics, whereas the net growth and sinking terms determine population dynamics based on phytoplankton physiology. Phytoplankton physiology is defined by a multiplicative formulation (2.21) with component terms discussed in Appendix B.

$$g_{net}(I,N,P,Si,T) = g_{\max} f(I) h(T) \min(l(N), l(P), l(Si)) - r - Z_{graze} \quad (2.21)$$

Where g_{max} is the maximum growth rate, f(I) is light limitation, h(T) is temperature limitations, l(N), l(P), and l(Si) are nitrogen, phosphorous, and silica limitations, r is respiration, and Z_{graze} is zooplankton grazing. The multiplied equations will be referred to as the multiple growth factor ($m_F = f(I)h(T)\min\left(l(N)l(P)l(Si)\right)$).

Photosynthesis was represented by (2.22) (Platt, Gallegos, and Harrison, 1980). Temperature was represented by a Gaussian model used by Cerco and Seitzinger (1997) (2.23). Nutrients were represented by a simple Michaelis-Menton model (2.24) (Thomann and Mueller, 1987). Respiration and zooplankton grazing are based on first-order kinetics with zooplankton grazing described by (2.25) (Thomann and Mueller, 1987).

$$g_{\max} f(I(z,t)) = g_{\max}\left(\frac{\alpha+\beta}{\alpha}\right)\left(\frac{\alpha+\beta}{\beta}\right)^{\frac{\beta}{\alpha}}\left[\left(1-e^{-\alpha I(z,t)}\right)e^{-\beta I(z,t)}\right] \quad (2.22)$$

$$I(z,t) = I_o(t)\exp(-k_z z)$$

Where f(I(z)) is the normalized form given in Appendix B, α=0.00132, β=0.00136, I_o is the incident solar radiation, k_d is the light attenuation coefficient, z is depth, and t is time.

$$h(T(z,t)) = \exp(-0.0067(T(z,t)-17.3)^2) \quad when \quad T(z,t) \le 17.3$$
$$h(T(z,t)) = \exp(-0.012(17.3-T(z,t))^2) \quad when \quad T(z,t) \ge 17.3 \quad (2.23)$$

Where T is ambient water temperature (^oC).

$$l(N(t)) = \frac{N(t)}{K_N + N(t)} \qquad (2.24)$$

Where K_N is the half-saturation constant and N is the nitrogen concentration; similarly for phosphate (P) and silica (Si).

$$Z_{graze} = F_Z Z(t) \tag{2.25}$$

Where F_Z is the filtering rate per animal and Z is number of animals per unit volume.

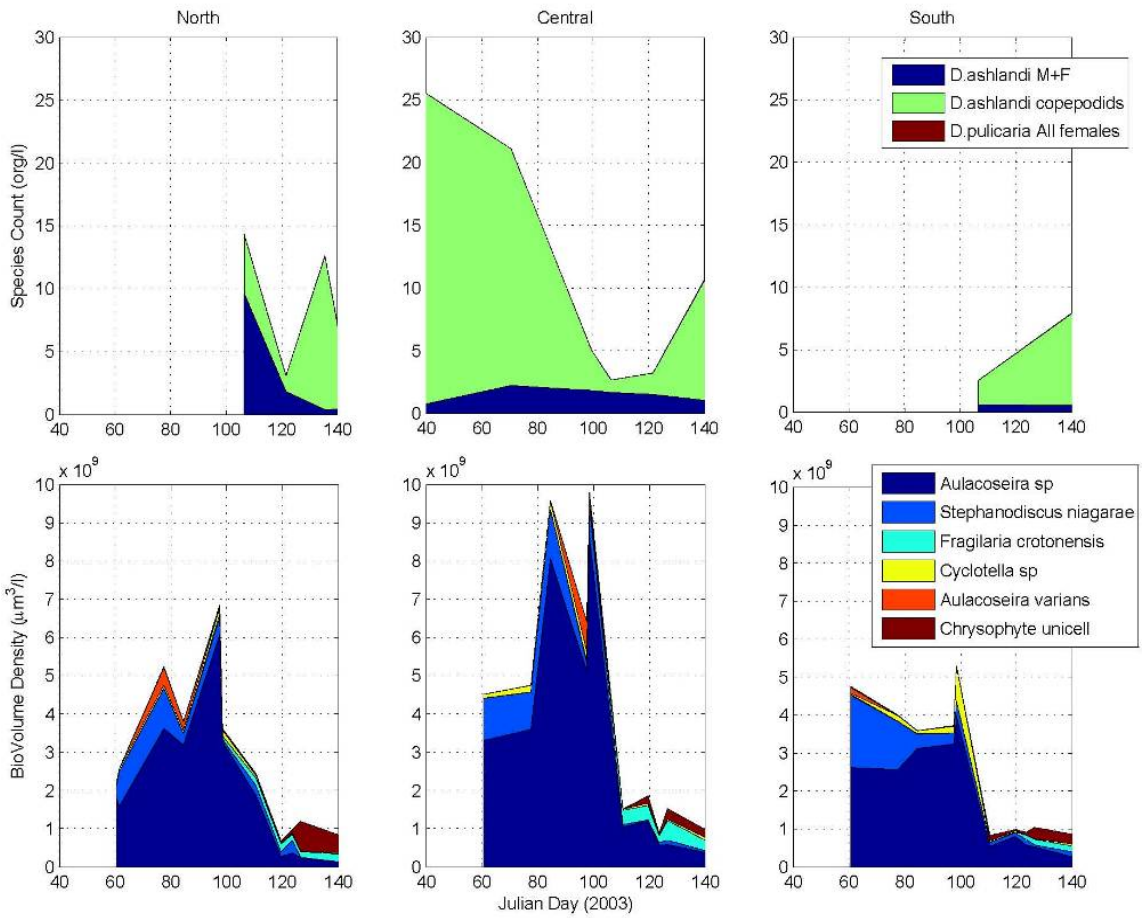

Figure 2. 6. Most abundant species that comprised the zooplankton (upper panels) and phytoplankton (lower panels) populations for year 2003. Note, org/l is organisms/liter. The zooplankton count is the average from zero to 20 meters.

2.3 Field Results

2.3.1 Observed Plankton Densities

During the early-spring period for the years 2003 and 2004, phytoplankton and zooplankton species observations were similar (Figure 2. 6 and Figure 2. 7). *Aulacoseira subarctica* was the most significant species (by biovolume density) for 2003, but in 2004 *Stephanodiscus niagarae* was the most significant species and *A. subarctica* was the second most significant. *Diaptomus (Leptodiaptomus) ashlandi* copepodids and adults were the most abundant animals in both years. For the two years, temporal developments were similar: the phytoplankton bloom started around JD 80 and lasted for approximately 20 days. In the central portion of the lake,

zooplankton copepodids showed two peaks whereas the adults showed a single peak that occurred after the phytoplankton peak in 2004, which was a more typical response observed by Edmondson and Litt (1982) and a classic predator/prey behavior (Arhonditsis and Brett, 2005a and 2005b). Spatial distributions were also similar for both years.

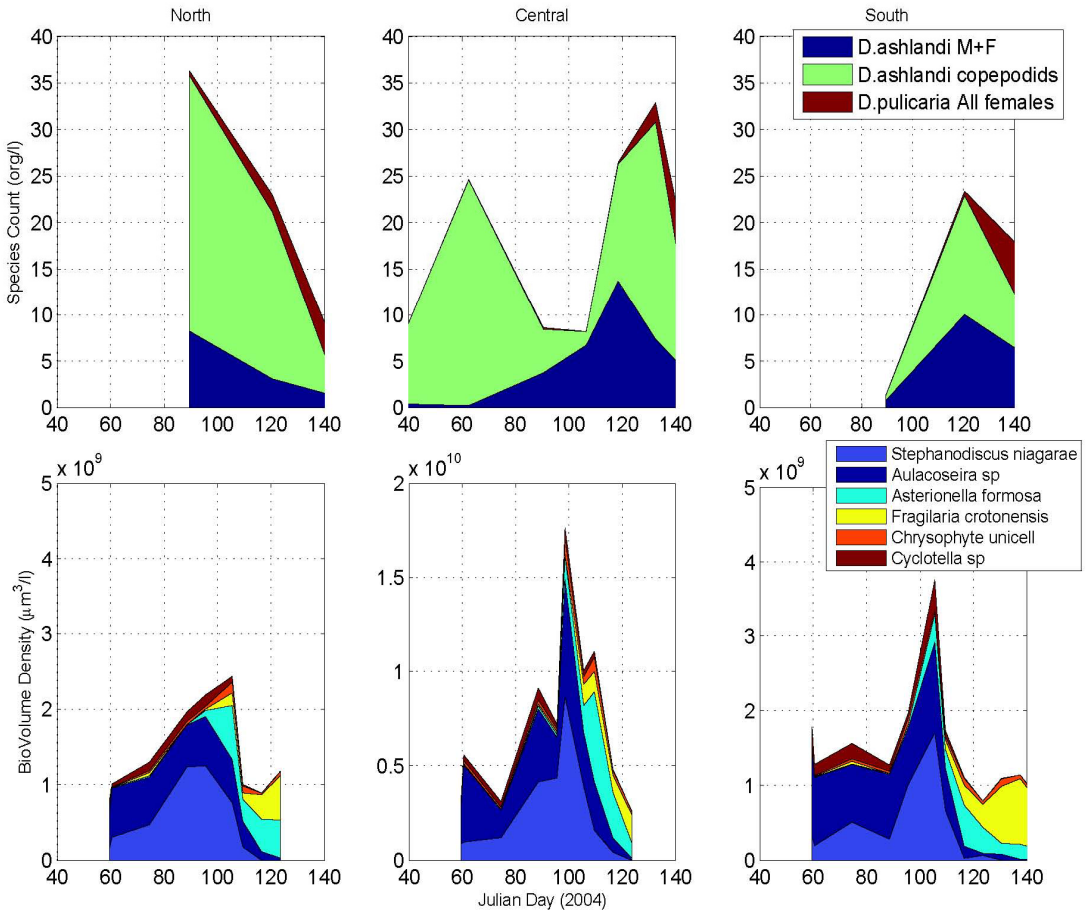

Figure 2. 7. Most abundant species that comprised the zooplankton (upper panels) and phytoplankton (lower panels) populations for year 2004 (note the larger scale for the central phytoplankton). The zooplankton count is the average from zero to 20 meters.

For both years, phytoplankton biovolumes were highest in the central portion of the lake, with the north and south portions having lower densities. For the zooplankton, 2004 densities appeared to be the highest in the north portion early in the year with higher densities shifting to the central portion as the bloom progressed. A similar pattern may have existed in 2003, but both patterns are difficult to affirm because of the late sampling dates. For both years in the central portion, bloom development

occurred as copepodids densities declined, but in 2004 at the north end, the phytoplankton and zooplankton populations appeared to be synchronized; this condition may have occurred in 2003 because phytoplankton and zooplankton concentrations appear to decrease together between JD 100 and 120.

2.3.2 Measured Particle and Phytoplankton Concentrations

The quantitative phytoplankton results represent average conditions in the upper ten meters. I make the case that particle measures from the LISST-100 are an effective surrogate for vertical distributions of the phytoplankton community; the LISST-100 has been successfully applied to assess phytoplankton and bacteria concentrations and distributions (Serra et al., 2001; Serra et al., 2003).

The LISST-100 measured particle diameters from 2.5 to 500 µm and records the median particle size from 2.73 to 462 µm with size increasing at 1.18 times the lower size (i.e., equal change in class size in log(size) space) for a total of 32 classes. To reduce the data set and smooth the observations, we averaged the data into four classes (Table 2. 1). The classes were selected because observations suggested particle sizes tended to group within the four ranges and because *A. subarctica* and *S. niagarae* cell dimensions lie within these ranges (Table 2. 2). For the four groups, mean particle concentration was calculated over the upper ten meters and compared to observed *A. subarctica* and *S. niagarae* biovolume concentrations, which sampled the upper ten meters of the water column.

Table 2. 1. Reduction of particle sizes into four representative groups; each group represents a range of diameters.

Mean Diameter (µm)	Diameter Group (µm)
5	3.8, 4.5, 5.3, 6.2
16	10.3, 12.1, 14.3, 16.9, 19.9, 23.5
75	63.4, 74.8, 88.3
119	88.3, 104, 123, 145

The 5 and 16 µm particles tracked phytoplankton biovolume better than the two larger sizes, which continuously increased over the study period (Figure 2. 8 and Figure 2. 9). The 75 and 119 µm group may track the evolution of *Asterionella formosa* and *Fragilaria crontonensis* (Table 2. 2), which showed increasing biovolume concentrations after the decline in *A. subarctica* and *S. niagarae* (Figure 2. 7 and Figure 2. 9). LISST particle concentrations were considerably less than the

phytoplankton biovolume concentration, and the MWY observations did not show higher concentrations compared to NOA and SWA (Figure 2. 10). Particle size and concentration differences most likely result from the cylindrical phytoplankton shape compared to the spherical shape assumed by the LISST, which measures particle diameter by laser diffraction principles induced for a sphere.

Table 2. 2. Typical cell dimensions for *A. subarctica* and *S. niagarae*; *Asterinonella formosa* and *Fragilaria crotonensis* are also presented.

Species (shape)	Length per cell (µm)	Diameter (µm)
A. subarctica (cylinder)[(1)(2)]	15-24 (up to 10 cells per chain)	4-14
S. niagarae (cylinder)[(3)]	21	33
Asterionella formosa[(1)]		130(8 cells)
Fragilaria crotonensis[(1)]		70(10 cells)

(1) Reynolds, 1983
(2) Gibson et al., 2003
(3) Infante and Litt, 1985

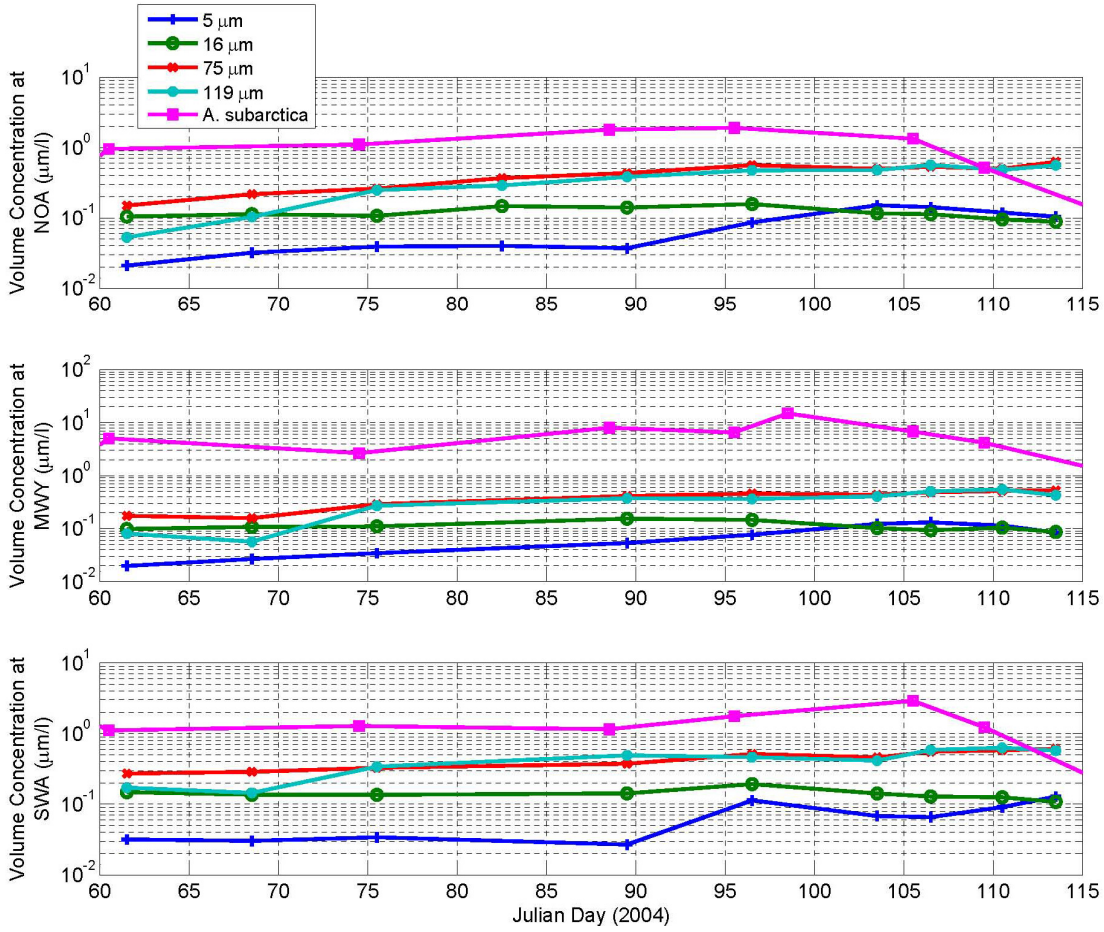

Figure 2. 8. Measured LISST particle and phytoplankton biovolume concentrations at NOA, MWY, and SWA for year 2004. The 75 and 119 µm particle concentration increased with time while the 5 and 16 µm tracked more with the *A. subarctica* concentrations. Note scale change for MWY.

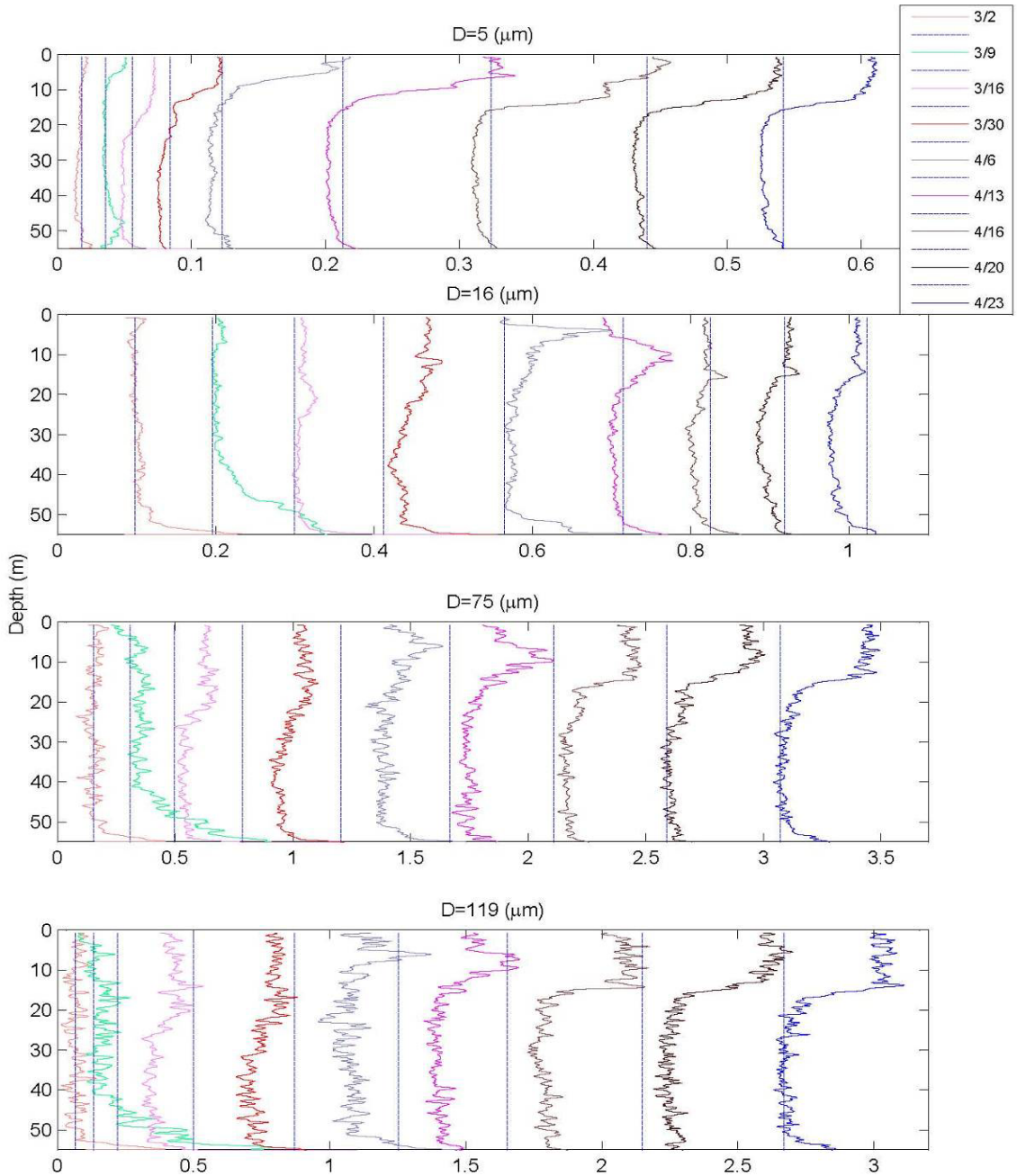

Figure 2. 9. Temporal evolution of the four particle groups at MWY for year 2004; NOA and SWA had similar results. Each profile is proportionally offset from the previous observation based on a cumulative concentration. Each profile is related to the initial concentration by the vertical blue line, which represents the depth average concentration for the first profile taken March 2, 2004.